Research Article | Vol. 11, No. 2 / 1 February 2021 / Optical Materials Express 425
Optical Materials EXPRESS

Anisotropic circular topological structures

LAURA PILOZZI[1,*] AND CLAUDIO CONTI[1,2]

[1] Institute for Complex Systems, National Research Council (ISC-CNR), Via dei Taurini 19, 00185 Rome, Italy
[2] Department of Physics, University Sapienza, Piazzale Aldo Moro 5, 00185 Rome, Italy
[*] laura.pilozzi@isc.cnr.it

Abstract: We design cylindrical multilayer structures characterized by anisotropy and topological features. This provides a new approach to tailor electromagnetic fields into desired patterns with orbital angular momentum in cylindrical geometries as ring resonators and fibers. We use transformation optics to deal with anisotropic circular structures, and rigorously define the edge states. The resulting topologically protected high-localized modes, at the core/cladding interface, with angular momentum may trigger the developments of new disorder-robust devices and high Q-microcavities for applications in light transmission, quantum technology, nonlinear optics, TeraHertz devices, and biophysical sensors.

1. Introduction

Over the past 20 years a plethora of unusual effects on light propagation has been obtained designing structures that gain their properties from a given pattern [1]. New and enhanced features have been achieved with these synthetic materials realizing permittivities and permeabilities not available in nature, for example implementing anisotropy by design [2,3].

Concurrently, the rapidly grown branch of topological photonics has featured novel fundamental concepts for a more effective control of light behavior. Through topological metamaterials, allowing nontrivial wave propagation, many breakthroughs have been achieved as backscattering-free edge states [4], topological polaritons [5], topological lasing [6–8] and the generation of synthetic gauge fields in synthetic dimensions [9], to cite a few.

For the description of the combined effects of anisotropy and topology, transformation optics [10], which exploits the equivalence between media with spatially varying optical response and curved spacetime, turns out to be a useful technique that we here apply to model topological optical resonators [11] in cylindrical geometry.

Structures with anisotropic and radial dependent constitutive parameters [12,13] are known to support Fabry-Perot, cavity and whispering gallery modes. We show that, by a proper modulation of geometry and refractive index distribution, one can obtain, additionally, radial edge states protected by topology. We indeed find strongly localized modes, at the core/cladding interface, with non-vanishing optical angular momentum. In these modes, scattering due to defects or disorder is inhibited. This property enables a robust and scalable design, and opens the way to ultra-high Q resonators for many applications from optics to microwaves. Remarkably, the use of topological concepts and transformation optics enables a rigorous design of the devices. The proposed resonator, shown schematically in Fig. 1(a), has an homogeneous and isotropic core and a cladding given by a sequence of pairs of layers 'a' and 'b' characterized by dielectric and magnetic tensors $\overleftrightarrow{\epsilon}_\alpha$ and $\overleftrightarrow{\mu}_\alpha$ with $\alpha = a, b$. As a prototypical model, allowing for nontrivial topological phases, we consider a cosine modulation of its radial geometrical parameters in the form of the Aubry-Andre-Harper (AAH) model [14]. Specifically, the centers positions of the 'a' layers, s_a wide, are given by $\rho_n^a = d_o \left[n + \eta\delta_n^H\right]$, where $\delta_n^H = \cos(2\pi\gamma n + \phi)$ is the Harper modulation [14] and η is a coefficient that controls its strength. In the ρ direction, the cladding is a periodic structure with q 'a' layers in the unit cell and a period $d = qd_o$, where d_o is the period

#412528 https://doi.org/10.1364/OME.412528
Journal © 2021 Received 14 Oct 2020; revised 26 Nov 2020; accepted 4 Dec 2020; published 21 Jan 2021

Optical Materials EXPRESS

of the unmodulated structure ($\eta = 0$). The phase $\phi \in (0, 2\pi)$, the topological parameter of the 1D periodic modulation, adiabatically deforms the system and accounts for the momentum along the second geometrical dimension of its 2D ancestor lattice [15,16]. This phase then encodes a synthetic dimension of our system and dictates the trivial or non-trivial character of the gaps and then the presence of edge modes. The 2D "ancestor" system exhibits broken time inversion symmetry [16] that can be interpreted as the presence of an effective magnetic field and gives protection against backscattering.

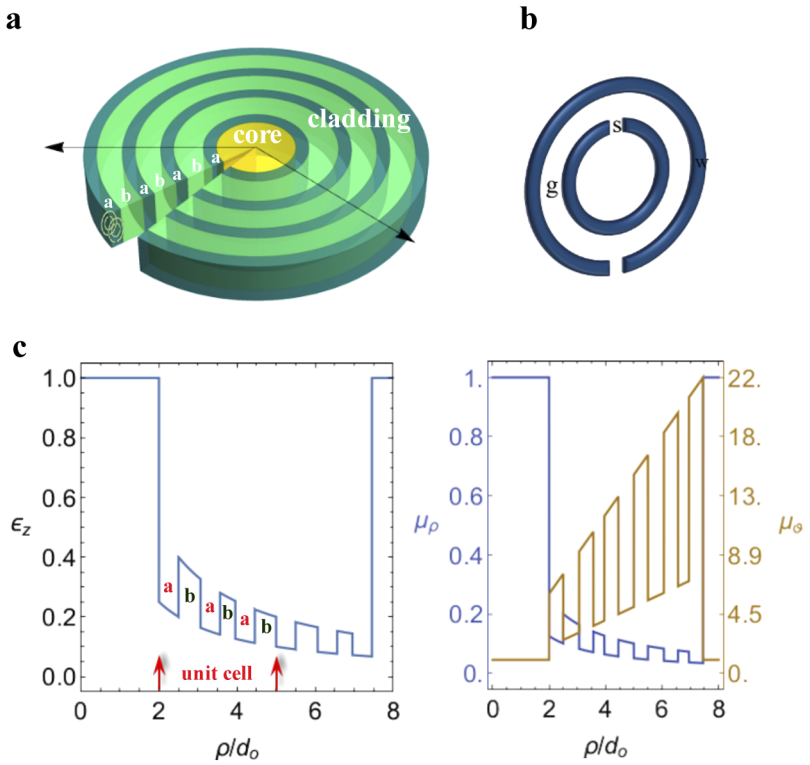

Fig. 1. Schematic representation of a) the topological optical resonator and b) a split-ring resonator(SRR). c) Constitutive parameters of the topological optical resonator for $\phi = 0.5\pi$, $\tilde{\epsilon}_{z_a} = 1/1.5, \tilde{\epsilon}_{z_b} = 1, \tilde{\mu}_{\rho_a} = 0.25, \tilde{\mu}_{\rho_b} = 0.5, \tilde{\mu}_{\theta_a} = 2, \tilde{\mu}_{\theta_b} = 1$. The first two periods of the cladding are shown with $s_a = 0.5d_o$ and a core radius $\rho_c = 2d_o$.

The radial dependent dielectric and magnetic tensors $\overleftrightarrow{\epsilon}_\alpha$ and $\overleftrightarrow{\mu}_\alpha$ can be practically implemented by the use of artificially structured materials. An example [17] is to design the unitary cell of each layer with, as basic building blocks, split ring resonators (SRRs) [18]. Different geometries, as rings, squares, s-shaped or omega loops, have been proposed but, essentially, as shown in Fig. 1(b), the basic topology of a SRR consists of a pair of enclosed metallic loops, w wide, on a dielectric substrate, separated by a gap (g) and with splits (s) in them at opposite ends. By designing its parameters it is possible to achieve a target operating frequency [19,20]. Two schematic SRRs are shown in Fig. 1(a) to show the structuring of the annular layers.

Optical Materials EXPRESS

2. Methods

To design the topological structure of Fig. 1(a) we consider Maxwell equations, for diagonal tensors, in a generalized orthogonal coordinates (ξ^i) system [21]:

$$\begin{cases} \omega^2 h_k E_k = \frac{1}{\tilde{\epsilon}_k}\{\frac{\partial}{\partial\xi^i}\frac{1}{\tilde{\mu}_j}[\frac{\partial}{\partial\xi^k}(h_i E_i) - \frac{\partial}{\partial\xi^i}(h_k E_k)]+ \\ -\frac{\partial}{\partial\xi^j}\frac{1}{\tilde{\mu}_i}[\frac{\partial}{\partial\xi^j}(h_k E_k) - \frac{\partial}{\partial\xi^k}(h_j E_j)]\} \\ \omega^2 h_k H_k = \frac{1}{\tilde{\mu}_k}\{\frac{\partial}{\partial\xi^i}\frac{1}{\tilde{\epsilon}_j}[\frac{\partial}{\partial\xi^k}(h_i H_i) - \frac{\partial}{\partial\xi^i}(h_k H_k)]+ \\ -\frac{\partial}{\partial\xi^j}\frac{1}{\tilde{\epsilon}_i}[\frac{\partial}{\partial\xi^j}(h_k H_k) - \frac{\partial}{\partial\xi^k}(h_j H_j)]\} \end{cases} \tag{1}$$

where we have made use of the invariance with respect to transformations conserving simultaneously the values for $x_\ell h_i h_j / h_\ell \equiv \tilde{x}_\ell$ with $x = \epsilon, \mu$ and h_i the Lamé coefficients.

Specifically, in cylindrical coordinates $(\xi^1, \xi^2, \xi^3) = (\rho, \theta, z)$ and $(h_1, h_2, h_3) = (1, \rho, 1)$. Moreover, given the invariance of the material properties with respect to the z direction, the structure's axis, Eq. (1) reduces to:

$$\begin{cases} \omega^2 E_z = -\frac{1}{\epsilon_z \rho}\{\frac{\partial}{\partial\rho}\frac{\rho}{\mu_\theta}\frac{\partial}{\partial\rho}E_z + \frac{\partial}{\partial\theta}\frac{1}{\mu_\rho \rho}\frac{\partial}{\partial\theta}E_z\} \\ \omega^2 H_z = -\frac{1}{\mu_z \rho}\{\frac{\partial}{\partial\rho}\frac{\rho}{\epsilon_\theta}\frac{\partial}{\partial\rho}H_z + \frac{\partial}{\partial\theta}\frac{1}{\epsilon_\rho \rho}\frac{\partial}{\partial\theta}H_z\} \end{cases} \tag{2}$$

so that the choice:

$$[x_\rho(\rho), x_\theta(\rho), x_z(\rho)] = [\frac{1}{\rho}\tilde{x}_\rho(\rho), \rho\tilde{x}_\theta(\rho), \frac{1}{\rho}\tilde{x}_z(\rho)]$$

for the radial dependence of the dielectric tensors, with $\tilde{x}_\ell(\rho)$ periodic functions, makes the differential operator in Eq. (1) invariant under translations of the form $\rho \longrightarrow \rho + nd$.

Writing every field component in the form $\psi(\rho, \vartheta, z, t) = \psi(\rho, \vartheta)e^{i(\beta z - \omega t)}$, for $\beta = 0$ (*i.e.* a two dimensional system), in each of the cladding layers, where $\tilde{x}_\alpha(\rho) = \tilde{x}_{\alpha_j}$, one then has:

$$\begin{bmatrix} \frac{\partial^2}{\partial\rho^2} + (\omega^2\tilde{\epsilon}_{z_j}\tilde{\mu}_{\theta_j} - \frac{\tilde{\mu}_{\theta_j}}{\tilde{\mu}_{\rho_j}}\ell^2) \end{bmatrix} E_z^j = 0 \\ \begin{bmatrix} \frac{\partial^2}{\partial\rho^2} + (\omega^2\tilde{\mu}_{z_j}\tilde{\epsilon}_{\theta_j} - \frac{\tilde{\epsilon}_{\theta_j}}{\tilde{\epsilon}_{\rho_j}}\ell^2) \end{bmatrix} H_z^j = 0 \tag{3}$$

They show that a renormalization of the constitutive parameters, represented in Fig. 1(c), allows to map a region with curvilinear boundaries, filled with a radial dependent anisotropic material, into an equivalent planar region. Equations (3) then, have plane-wave solutions with dispersion relations for TE and TM polarizations given by:

$$k^2_{i\ell_{te}} = \omega^2\tilde{\epsilon}_{z_j}\tilde{\mu}_{\theta_j} - \frac{\tilde{\mu}_{\theta_j}}{\tilde{\mu}_{\rho_j}}\ell^2 \\ k^2_{i\ell_{tm}} = \omega^2\tilde{\mu}_{z_j}\tilde{\epsilon}_{\theta_j} - \frac{\tilde{\epsilon}_{\theta_j}}{\tilde{\epsilon}_{\rho_j}}\ell^2 \tag{4}$$

The electric field inside each layer in the cladding can then be expressed as the sum of a left- and a right-traveling wave:

$$\begin{bmatrix} E_z^j \\ H_z^j \end{bmatrix} = (\overleftrightarrow{E}_{pj}\,\vec{a}_j + \overleftrightarrow{E}_{mj}\,\vec{b}_j)e^{i\ell\theta} \quad \text{for} \quad \rho_1 < \rho < \rho_N \tag{5}$$

Optical Materials EXPRESS

where:

$$\overleftrightarrow{E}_{pj} = \begin{bmatrix} e^{ik_{j\ell_{te}}(\rho-\rho_{j-1})} & 0 \\ 0 & e^{ik_{j\ell_{tm}}(\rho-\rho_{j-1})} \end{bmatrix}$$

and $\overleftrightarrow{E}_{mj} = \overleftrightarrow{E}_{pj}^{-1}$.

Fields in two consecutive layers are related through the boundary conditions requiring the continuity of the longitudinal field components (E_z^j, H_z^j) and of the transverse one:

$$(E_\theta^j, H_\theta^j) = (-\frac{i}{\omega\tilde{\epsilon}_{\theta j}\rho}\frac{\partial}{\partial\rho}H_z^j, \frac{i}{\omega\tilde{\mu}_{\theta_j}\rho}\frac{\partial}{\partial\rho}E_z^j) \tag{6}$$

Moreover, being $\tilde{x}_\alpha(\rho)$ periodic quantities, one can apply Bloch's theorem to obtain the photonic band structure. Given the transfer matrix $T^{(1)}(\omega)$ for the single period of the cladding, the photonic bands are then obtained by: $2cos(Kd) = Tr[T^{(1)}(\omega)]$.

3. Results

Mode's dispersions for TE polarization are shown in Fig. 2 for an unmodulated cladding ($\eta = 0$); all the modes with $\ell \neq 0$ have a cut-off frequency. Moreover the optical tensors values define gap widths and modes reciprocal positions for different ℓ values.

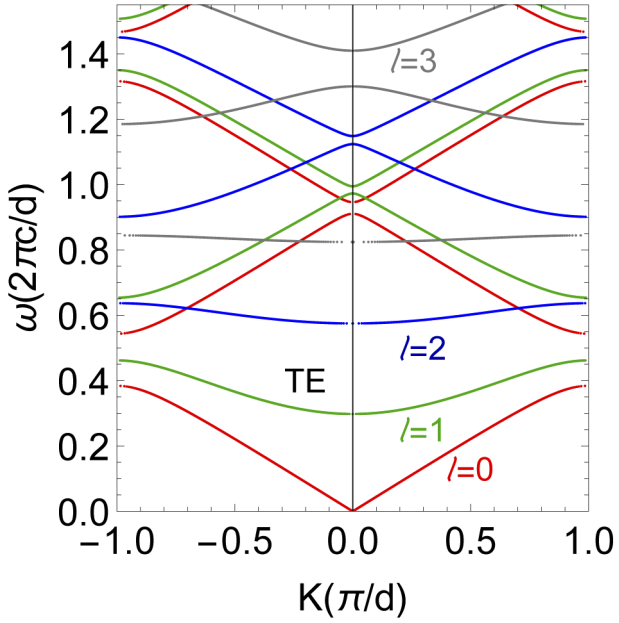

Fig. 2. TE dispersion curves for the anisotropic circular resonator with a periodic unmodulated cladding; K is the Bloch wave vector.

Adding the modulation, *i.e.* for a cladding with $\eta \neq 0$, Fig. 3 shows, with blue lines, how mode's dispersion modifies. A comparison with the dispersion for the unmodulated cladding (green curves) indicates the opening of mini-gaps (yellow regions) that, due to the peculiar modulation δ_n^H of the cladding, are topologically non-trivial *i.e.* present a twisting of the band structure. Indeed, as shown in Fig. 4 for the modes $l = 0$ and $l = 1$, states are present bridging the mini-gaps as the phase ϕ is varied, a sign of the bands swapping. Similarly to the modes of a planar isotropic structure, these states are localized at the edge of the anisotropic cladding and add

Optical Materials EXPRESS

to the set of possible resonances associated with radial photonic structures [12,13]. Specifically, the projected dispersions in Fig. 4 show gaps (empty regions) and bands (filled blue regions) for the anisotropic resonator and, with solid lines, the modes localized at the core/cladding interface. Given the symmetry of the cladding [22] with respect to the phase $\chi = \phi + \pi/\gamma - \pi/2$, the dashed lines give again the modes localized at the core edge but for a structure with an inverted sequence ($\chi \rightarrow -\chi$ in δ_n^H) of the layers in the cladding.

To show the localization we study the electric field pattern specific for each mode. In the homogeneous and isotropic innermost (j=1) and outermost (j=N+1) layers the longitudinal field components can be represented by a linear combination of the Hankel functions of the first and second kind:

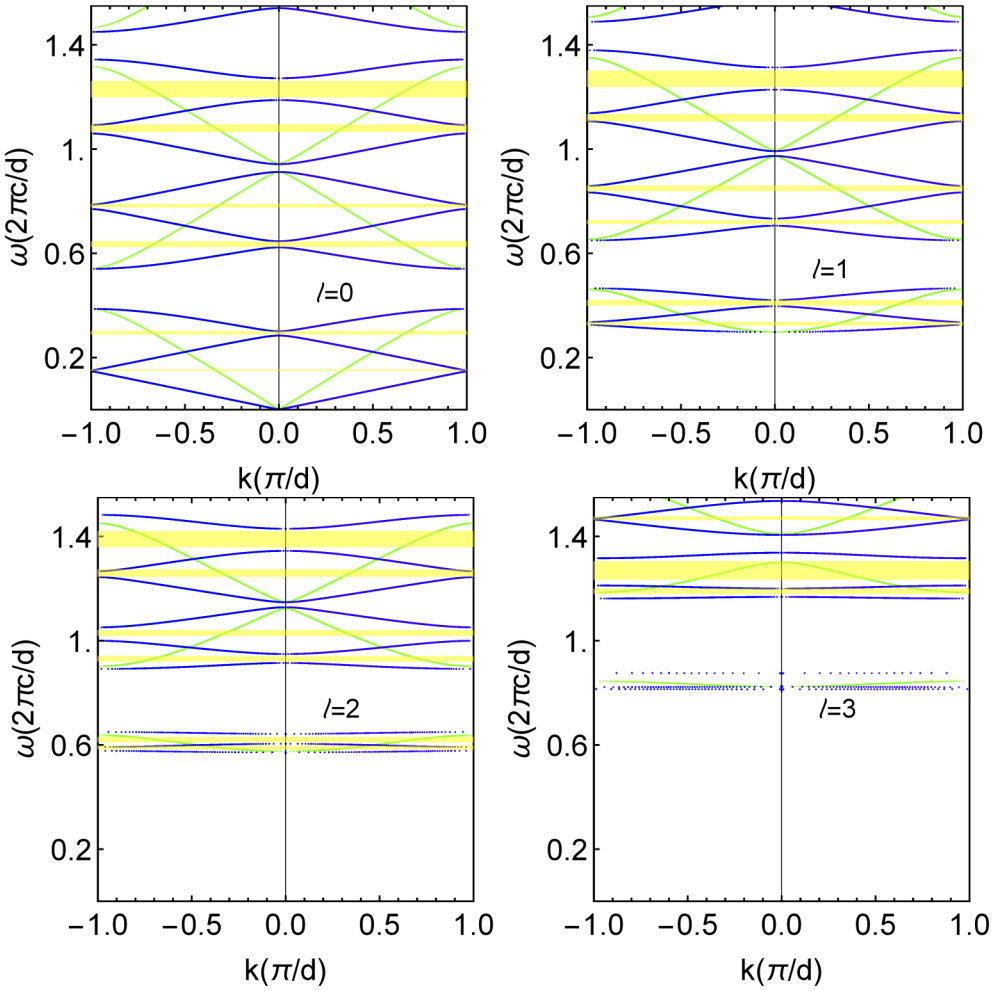

Fig. 3. TE dispersion curves for the anisotropic circular resonator with a periodic unmodulated cladding (green curves) and a periodic modulated cladding (blue curves) for different ℓ values. K is the Bloch wave vector. Yellow colored regions indicate the non-trivial gaps.

for $0<\rho<\rho_c$:

$$E_z^1 = H_\ell^{(1)}(k_1\rho) + H_\ell^{(2)}(k_1\rho) r_{te}$$
$$H_\theta^1 = \frac{i}{\omega\mu_1\rho}\left[\dot{H}_\ell^{(1)}(k_1\rho) + \dot{H}_\ell^{(2)}(k_1\rho) r_{te}\right] \quad (7)$$

Optical Materials EXPRESS

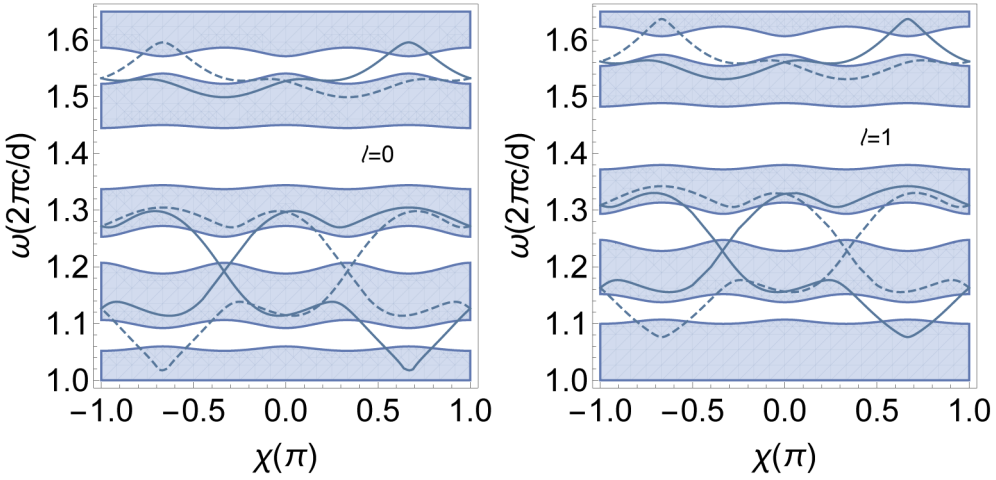

Fig. 4. Projected dispersions showing gaps (empty regions) and bands (filled regions) for the anisotropic resonator for modes with $\ell = 0, 1$. Full curves give the dispersions of edge modes localized at the core/cladding interface. Dashed curves give edge modes for a cladding with an inverted modulation: $\chi \rightarrow -\chi$ in δ_n^H.

for $\rho > \rho_N$:

$$\begin{aligned} E_z^{N+1} &= H_\ell^{(1)}(k_{N+1}\rho)t_{te} \\ H_\theta^{N+1} &= \frac{i}{\omega\mu_{N+1}\rho}\left[\dot{H}_\ell^{(1)}(k_{N+1}\rho)t_{te}\right] \end{aligned} \tag{8}$$

where $k_i = \omega\sqrt{\epsilon_i\mu_i}$ for $i = 1, N+1$ while, r_{te} and t_{te} are the reflectivity and transmittivity coefficients.

Then the boundary conditions between adjacent cylindrical layers allow to show that, as long as the modulation strenght η is null, possible modes are:

- Fabry-Perot modes, located in the cladding;
- cavity modes existing in the core;
- whispering gallery modes localized at the outer boundary of the structure.

Interestingly, for a modulation strenght $\eta \neq 0$, at the frequencies of edge states an additional field localization can be obtained at the cladding/core interface.

Fields in the whole structure are obtained by the standard transfer matrix method [23] trough a product of matrices relating the field amplitudes in consecutive layers. The elements of these 2x2 matrices are obtained by requiring the continuity of the longitudinal and transverse field components, at the core/cladding interface by using Eq. (7) and at the cladding/external medium by using Eq. (8). In the N periods of the cladding region, where we can apply the Bloch's theorem, the matrix that transfer the field from the first to the last layer is simply given by the N-th power of the single period matrix $T^1(\omega)$.

Following Ref. [24], field profiles are shown in Figs. 5(a)–5(d) for a cylindrical resonator with a multi-annular unmodulated cladding ($\eta = 0$) with the geometrical and optical parameters given in Fig. 1(c). Specifically, these figures give the profiles for Fabry-Perot, cavity and whispering-gallery modes. They are the typical resonances of a wave field in a resonator.

The localization of the edge modes at the core/cladding interface is shown in Figs. 5(e)–5(g) for a structure with a δ_n^H-modulated cladding with $\chi = -0.4\pi$, for different l values. The

Optical Materials EXPRESS

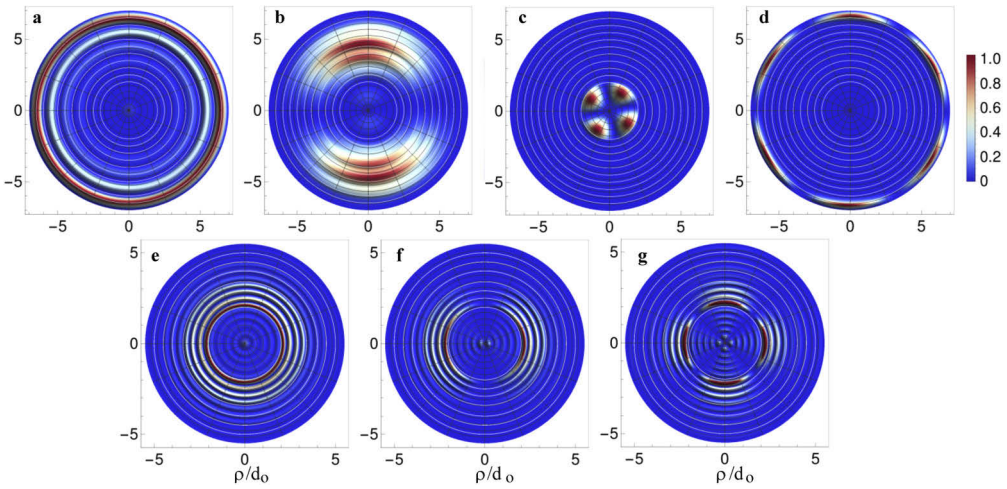

Fig. 5. Normalized electric field pattern for the resonant structure: a) whispering-gallery mode for $\ell = 0$, $\omega(2\pi c/d) = 0.472$ b) Fabry-Perot mode for $\ell = 1$, $\omega(2\pi c/d) = 0.310$ c) cavity mode for $\ell = 2$, $\omega(2\pi c/d) = 0.316$ d) whispering-gallery mode for $\ell = 3$, $\omega(2\pi c/d) = 0.944$; edge modes for e) $\ell = 0$, $\omega(2\pi c/d) = 1.23$, f) $\ell = 1$, $\omega(2\pi c/d) = 1.27$, g) $\ell = 2$, $\omega(2\pi c/d) = 1.38$.

frequencies of these edge modes lay in non-trivial gaps and, for the value $\chi = -0.4\pi$, are $\omega(2\pi c/d) = 1.23, 1.27, 1.38$ respectively for the different l modes

These figures show that the combined effect of anisotropy and topology may drive cylindrical structures into a topological phase, where high-localized modes, at the core/cladding interface, with angular momentum may trigger the development of new structures with additional functionalities.

Indeed we propose a scheme to create localized modes by the implementation of a topological interface in a radial structure. In this 2D system the topological interface consists of a boundary line separating two distinct topologically ordered regions, specifically the core and the cladding, where non-chiral protected edge modes are located and propagate. Indeed, the $\pm\ell$ modes are degenerate due to the ℓ^2 term in Eq. (3).

The peculiar origin of these modes, the bulk-edge correspondence [25], gives them characteristic properties with respect to other localized modes, as for example whispering gallery modes, present in the same structure. They include controllable features as the position, the localization length and the quality factor. First of all, we remind that the general bulk-edge correspondence states that any interface separating two topologically different regions of space necessarily hosts topologically protected edge modes.

Our scheme exploits the radial core/cladding interface but suggests the possibility of engineering a topological interface within the cladding. By spatially varying the cladding modulation, which indeed split it into topologically distinct regions, one can achieve the possibility of tuning the edge mode position. Differently, whispering gallery modes (Fig. 5(d)) localize near a geodesic situated at the resonator boundary and are strongly affected by the external potential confinement.

As shown in Fig. 5, the edge states have a localization length of about four lattice sites for the parameters chosen in our calculations. This value, as well as the quality factor of the modes, which are a the order of 10^3, can be tuned by increasing the number of layers in the cladding, as happen in photonic crystal structures. Moreover, edge modes dispersions are located in the gap and this gives them protection against scattering into other modes.

Optical Materials EXPRESS

Actually, the narrowest mode in Fig. 5 appears in panel (d) and it is a whispering gallery mode. Nevertheless, being a resonant mode supported by continuous total internal reflection off the ring surface, it suffers from structure imperfections. Its intrinsic quality factor can indeed get contributions due to losses from many processes as scattering due to imperfections or bending that entails incomplete total internal reflection.

On the contrary, as they live in the gap's spectrum, edge states cannot be removed or added unless a topological transition of the bulk bands happens when the gap closes. This gives them a topological protection against radial disorder. By introducing a randomized perturbation of the A layers' center positions in the form $\rho_n^a = d_o \left[n + \eta\delta_n^H + \sigma\xi_n\right]$ where ξ_n are random variables chosen in the range $(-1; 1)$, while σ is the disorder strength, we observe a frequency variation of a specific mode of the order of 10^{-2} in reduced units.

Finally, edge states of a given angular momentum exhibit protection by resonant scattering into the allowed band with another angular momentum as long as coupling effects can be neglected. Resonant scattering among modes with different angular momentum is generally not present due to the lack of phase matching. Moreover the optical tensor values allow to tune the cut-off frequency, the gap widths and modes reciprocal positions for different angular momenta.

4. Conclusions

We have introduced and theoretically studied anisotropic circular structures, which sustain topological resonances in the form of edge states. Our findings demonstrate that judicious use of topology and anisotropy may open the way to new classes of devices. We have considered the cylindrical geometry for its potential impact in the design of waveguides, optical fibers, and resonators. Other geometries may be analyzed with the help of transformation optics, like spherical and conical systems. For the cylindrical case, our approach can rigorously define angular momentum in edge states and engineer the states at target frequencies and spatial configurations. This result may have an impact on the modern applications of topological photonics, as in quantum optics, where angular momentum can be used for multi-level quantum information processing, or in classical systems, for example in particle trapping and spectroscopy. Also, ring resonators are primarily studied for their many applications in nonlinear optics, as frequency comb generation for high precision measurements and metrology. We believe that the introduction of topological ideas, supported by a rigorous theoretical treatment, may introduce new opportunities because of the new design tools and robustness to disorder.

Funding. Sapienza Università di Roma (2017, 2016); Ministero dell'Istruzione, dell'Università e della Ricerca (2015KEZNYM NEMO, 20177PSCKT PELM); Horizon 2020 Framework Programme (820392); Horizon 2020 Framework Programme (731473).

Acknowledgments. The present research was supported by PRIN 2015 NEMO project (grant number 2015KEZNYM), H2020 QuantERA QUOMPLEX (grant number 731473), H2020 PhoQus (grant number 820392), PRIN 2017 PELM (grant number 20177PSCKT), Sapienza Ateneo (2016 and 2017 programs).

Disclosures. The authors declare no conflicts of interest.

References

1. D. R. Smith, J. B. Pendry, and M. C. K. Wiltshire, "Metamaterials and negative refractive index," Science **305**(5685), 788–792 (2004).
2. J. B. Pendry, A. J. Holden, D. J. Robbins, and W. J. Stewart, "Magnetism from conductors and enhanced nonlinear phenomena," IEEE Trans. Microwave Theory Tech. **47**(11), 2075–2084 (1999).
3. J. B. Pendry, A. J. Holden, D. J. Robbins, and W. J. Stewart, "Low frequency plasmons in thin-wire structures," J. Phys.: Condens. Matter **10**(22), 4785–4809 (1998).
4. Z. Wang, Y. Chong, J. D. Joannopoulos, and M. Soljacic, "Observation of unidirectional backscattering-immune topological electromagnetic states," Nature **461**(7265), 772–775 (2009).
5. T. Karzig, C.-E. Bardyn, N. H. Lindner, and G. Refael, "Topological polaritons," Phys. Rev. X **5**(3), 031001 (2015).
6. L. Pilozzi and C. Conti, "Topological lasing in resonant photonic structures," Phys. Rev. B **93**(19), 195317 (2016).
7. P. St-Jean, V. Goblot, E. Galopin, A. Lemaître, T. Ozawa, L. Le Gratiet, I. Sagnes, J. Bloch, and A. Amo, "Lasing in topological edge states of a one-dimensional lattice," Nat. Photonics **11**(10), 651–656 (2017).

Optical Materials EXPRESS

8. M. Parto, S. Wittek, H. Hodaei, G. Harari, M. A. Bandres, J. Ren, M. C. Rechtsman, M. Segev, D. N. Christodoulides, and M. Khajavikhan, "Edge-mode lasing in 1d topological active arrays," Phys. Rev. Lett. **120**(11), 113901 (2018).
9. A. Celi, P. Massignan, J. Ruseckas, N. Goldman, I. B. Spielman, G. Juzeliūnas, and M. Lewenstein, "Synthetic gauge fields in synthetic dimensions," Phys. Rev. Lett. **112**(4), 043001 (2014).
10. A. J. Ward and J. B. Pendry, "Refraction and geometry in maxwell's equations," J. Mod. Opt. **43**(4), 773–793 (1996).
11. L. Pilozzi, D. Leykam, Z. Chen, and C. Conti, "Topological photonic crystal fibers and ring resonators," Opt. Lett. **45**(6), 1415–1418 (2020).
12. D. Torrent and J. Sánchez-Dehesa, "Radial wave crystals: Radially periodic structures from anisotropic metamaterials for engineering acoustic or electromagnetic waves," Phys. Rev. Lett. **103**(6), 064301 (2009).
13. D. Torrent and J. Sánchez-Dehesa, "Acoustic resonances in two-dimensional radial sonic crystal shells," New J. Phys. **12**(7), 073034 (2010).
14. P. G. Harper, "The general motion of conduction electrons in a uniform magnetic field, with application to the diamagnetism of metals," Proc. Phys. Soc., London, Sect. A **68**(10), 879–892 (1955).
15. D. R. Hofstadter, "Energy levels and wave functions of bloch electrons in rational and irrational magnetic fields," Phys. Rev. B **14**(6), 2239–2249 (1976).
16. A. V. Poshakinskiy, A. N. Poddubny, L. Pilozzi, and E. L. Ivchenko, "Radiative topological states in resonant photonic crystals," Phys. Rev. Lett. **112**(10), 107403 (2014).
17. J. Carbonell, A. Díaz-Rubio, D. Torrent, F. Cervera, M. A. Kirleis, A. Piqué, and J. Sánchez-Dehesa, "Radial photonic crystal for detection of frequency and position of radiation sources," Sci. Rep. **2**(1), 558 (2012).
18. O. Sydoruk, E. Tatartschuk, E. Shamonina, and L. Solymar, "Analytical formulation for the resonant frequency of split rings," J. Appl. Phys. **105**(1), 014903 (2009).
19. R. Marques, F. Mesa, J. Martel, and F. Medina, "Comparative analysis of edge- and broadside- coupled split ring resonators for metamaterial design - theory and experiments," IEEE Trans. Antennas Propag. **51**(10), 2572–2581 (2003).
20. J. D. Baena, J. Bonache, F. Martín, R. M. Sillero, F. Falcone, T. Lopetegi, M. A. G. Laso, J. García-García, I. Gil, M. F. Portillo, and M. Sorolla, "Equivalent-circuit models for split-ring resonators and complementary split-ring resonators coupled to planar transmission lines," IEEE Trans. Microwave Theory Tech. **53**(4), 1451–1461 (2005).
21. L. S. Dolin, "To the possibility of comparison of three-dimensional electromagnetic systems with nonuniform anisotropic filling," Izv. VUZov Radiofizika **4**, 964–967 (1961).
22. A. V. Poshakinskiy, A. N. Poddubny, L. Pilozzi, and E. L. Ivchenko, "Radiative topological states in resonant photonic crystals," Phys. Rev. Lett. **112**(10), 107403 (2014).
23. W. C. Chew, *Waves and Fields in Inhomogeneous Media* (Van Nostrand Reinhold, New York, 1990).
24. A. Diaz Rubio, *Control of electromagnetic energy by metamaterials*, (2015).
25. G. M. Graf and M. Porta, "Bulk-edge correspondence for two-dimensional topological insulators," Commun. Math. Phys. **324**(3), 851–895 (2013).